Impact of measured spectrum variation on solar photovoltaic efficiencies worldwide

Geoffrey S. Kinsey[a], Nicholas C. Riedel-Lyngskær[b], Matthew Boyd[c], Marília Braga[d], Raul R. Cordero[e], Benjamin C. Duck[f], Christopher J. Fell[f], Sarah Feron[e], George Georghio[g], Atse Louwen[h], Takashi Minemoto[i], Ankit Mittal[j], Guilherme Neves[k], Gustavo Nofuentes Garrido[l], Basant R. Paudyal[m], Enio Bueno Pereira[k], Yves Poissant[n], Thomas Reindl[o], Marcus Rennhofer[j], Carlos D. Rodríguez-Gallegos[o], Ricardo Rüther[d], Wilfried van Sark[p], Miguel A. Sevillano-Bendezú[q], Jorge A. Tejero[l], Marios Theristis[r], Jan A. Töfflinger[q], Waldeir Amaral Vilela[k], Xiangao Xia[s], Márcia A. Yamasoe[t]

Abstract

In ratings of solar photovoltaic performance, variation in the spectrum of sunlight is commonly neglected. A single spectrum, AM1.5, is used as the sole basis not only for record laboratory efficiencies, but also for commercial module power ratings, the performance metrics for solar power plants, and product warranty claims. Incorporation of solar spectrum variation would improve accuracy and reduce the financial consequences of prediction errors. Ground-level measurements of spectral irradiance collected worldwide have been pooled to provide an extensive – though by no means comprehensive – sampling of the variation. Applied to nine solar cell types, the resulting divergence in solar cell performance illustrates that a single spectrum is insufficient for comparison of cells with different spectral responses. In contrast with single-junction cells such as silicon and cadmium telluride, cells with two or more semiconductor junctions tend to have efficiencies below that obtained under AM1.5. Increases in the degree of sun tracking are shown to decrease efficiency for cells with a narrower spectral response. Of the nine cell types, silicon exhibits the least spectral sensitivity: relative site variation ranges from 1% in Lima, Peru to 14% in Edmonton, Canada, with a mean of 4%.

Introduction

To anyone who has ever watched a sunset or gazed upon a deep blue sky, the idea of variation in the spectrum of sunlight is hardly surprising. Perhaps more surprising is the limited extent to which this variation is considered in solar photovoltaic operations. When comparing solar photovoltaic (PV) efficiencies, assessing generation of solar power plants, or evaluating performance warranty claims, a single standard spectrum (known as AM1.5, Appendix A) is the reference. While reliance on a single standard spectrum has had its advantages, including providing continuity over the years and consistency in results across academia and industry, the neglect of spectrum variation adds to uncertainty in solar energy generation[1–9]. Now that the lifetime costs of solar energy are dipping below those of fossil-fuel generation worldwide[10], variability in the solar resource is perhaps the last remaining (technical) obstacle to more rapid deployment. Accounting for spectrum variation will reduce prediction errors and cut one of the few remaining cords restraining the spread of solar energy generation.

Three parameters determine the efficiency of a solar photovoltaic cell: temperature, irradiance, and the spectrum of irradiance (the spectral irradiance)[11]. Temperature and (broadband) irradiance are routinely measured at solar installations and forecasted to determine grid availability of solar energy. Measurements of the third parameter, spectral irradiance, are considerably more sparse, conducted mostly by research groups. The power output of solar modules is rated using just a single spectrum and residential, commercial, and utility-scale PV systems are designed accordingly. For example, to determine if an operating solar power plant is meeting its contractual obligations, a key metric is the "performance ratio"[12]. This is calculated as the energy generated in a given time period divided by the (broadband) irradiance and the efficiency under the AM1.5 spectrum: any variation in the spectrum is neglected.

The AM1.5 reference spectrum was standardized in 1982[13] and concerns with over-reliance on it followed soon after [3,9,14,15]. Since that time, the information gap between spectral irradiance and temperature & broadband irradiance called out in [3] has persisted. Growth of the solar industry has led to temperature and broadband irradiance variation requirements being codified into international standards[16], data sheets[17], and warranty terms[18]. Meanwhile, the impact of spectral irradiance variation has often been treated as a secondary concern, or neglected[19]. The current international standard for solar module power rating defines four temperatures and four broadband irradiances, but only one spectrum[20]. The persistence of this gap is due partly to the perceived

expense in obtaining spectral irradiance measurements, as well as a legacy assumption that the relative impact on silicon, solar energy's workhorse material, is negligible.

As the solar market has risen well beyond €100 billion annually[21], and impending rapid climate change makes every kWh of renewable energy more precious, it is worth revisiting these assumptions. Variation of mere tenths of a percent now imply billions of euros gained or lost over the decades of operation - before the cost of carbon is included[22]. As detailed in [23], for a single 100-MW PV plant that displaces fossil-fuel generation, a 2% variation in operating performance is equivalent to about €150,000 in annual revenue and ~1,500 tons of avoided CO_2, or nine one-way flights between New York and Paris each year. As of 2021, the world has installed PV capacity equivalent to eight thousand such plants[24]. In the past two decades, as new solar cell designs using novel materials have proliferated[25], evidence for a need to incorporate spectral variation[4–6,26–56] has grown harder to ignore. However, given the limited amount of measured spectral irradiance data available, previous studies on its impact have had to rely on relatively small data sets, or synthetic spectra[5,23,39,57].
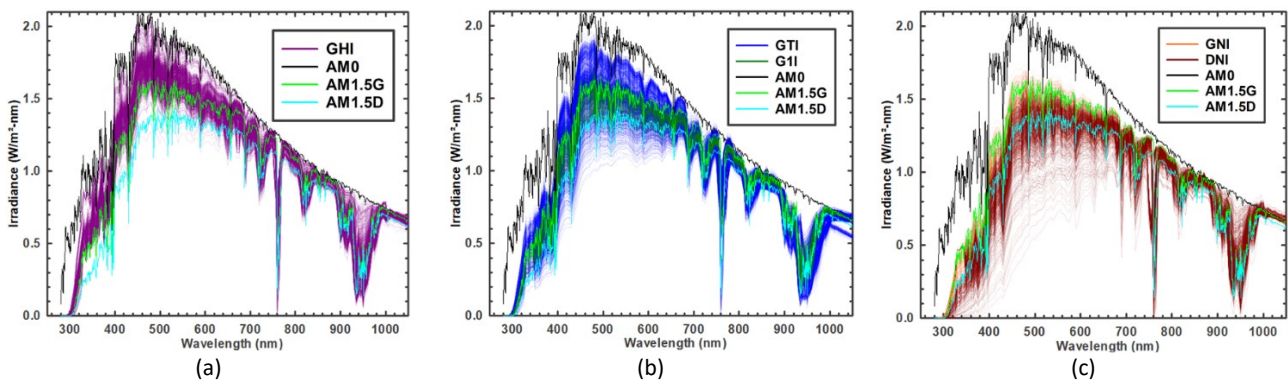

Figure 1. Spectral irradiance measured at the sites in Table 1: (a) global horizontal irradiance (GHI) (b) global tilt irradiance (GTI) and global one-axis irradiance (G1I); (c) global normal irradiance (GNI) and direct normal irradiance (DNI). Each line is a weekly sum of spectral irradiance sampled at 10-minute intervals (except for Chajnantor, CHL: 60-minute intervals). The spectra are normalized at either 880 nm or 1050 nm; AM1.5 values are substituted outside the measurement ranges. Standard spectra (AM0[58], AM1.5G, AM1.5D[59]) are shown for reference.

Measured spectral irradiance

A coalition of solar researchers has pooled their data from sites in Asia, Australia, Europe, and the Americas that span a range of latitudes, elevations, atmospheric conditions, and sensor orientations (Figure 1). Spectral irradiance is typically measured by spectroradiometers, instruments which employ optical diffraction to measure irradiance across a series of narrow wavelengths. A given diffractive optic can sample only a limited total wavelength range, so spectroradiometers for solar applications often measure wavelength ranges of around 300-1100 nm or 900-1700 nm[60] (Table 1). A pair of spectroradiometers spanning 300-1700 nm measures about 97% of the power in the extraterrestrial (AM0) spectrum[58]. An emerging alternative is to use a "solar spectral irradiance meter" that takes measured irradiance at a relatively small number of specific wavelengths as inputs to a model to reconstruct the full spectrum[61,62]. This is the instrument used for locations in Table 1 where the wavelength range is described as 280-4000 nm.

In parallel with direct measurement of ground-level spectral irradiance is the formulation of synthetic spectra. Synthetic spectra are formed by applying physical models using inputs of atmospheric properties (Appendix E)[8,63–67]. Limited site-level measurement of the atmospheric parameters is expanded using satellite remote sensing to produce synthetic spectra over extended geographic areas [66,67]. While synthetic spectra have demonstrated the ability to predict solar energy generation under a narrow set of field conditions[68–70], direct, ground-level measurements such as those presented here are needed to fine-tune the models and verify that the synthetic spectra remain accurate across the range of atmospheric conditions under which solar energy is generated worldwide. Synthetic spectra have previously been applied to analysis of the nine cell types in [23]. Differences between results from synthetic[66,67] and measured spectral irradiance are shown in Appendix E.

Spectral irradiance sensors can be mounted in orientations with varying degrees of solar tracking (Figure 1). Measurement of spectral irradiance has applications beyond solar PV, including monitoring of pollution[71] and

the radiative forcing arising from water vapor and other greenhouse gases[72,73]. As such, the most common orientation is horizontal, with the sensor exposed to the "global" spectrum arriving from the full hemisphere of the sky (global horizontal irradiance, "GHI"). For solar applications, preferred orientations are those that match the "plane of array" in which solar modules are mounted. The most common mounting orientation for PV modules is either a fixed tilt (global tilted irradiance, or "GTI") or one-axis tracking (global one-axis irradiance, "G1I"). Two-axis tracking keeps the surface perpendicular (normal) to the sun's rays and global normal irradiance ("GNI") is obtained. Finally, to capture irradiance coming only directly from the vicinity of the solar disc, two-axis tracking is combined with optics that exclude scattered sunlight for measurement of direct normal irradiance ("DNI").

The AM1.5 standard spectrum is defined for a wavelength range of 280-4000 nm[59]. Spectroradiometers measure only some portion of this range (Table 1). As detailed in Appendix B, for values outside the measurement range, AM1.5 values were substituted. The resulting spectra, grouped by mounting orientation, are shown in Figure 1. The spectrum for global horizontal irradiance (GHI), measured with sensors pointed upward at the dome of the sky is, not surprisingly, the "bluest". As the degree of solar tracking increases, the sensors begin to follow the sun to the horizons and irradiance shifts away from "blue" to the "red" and infrared; visible wavelengths (400-700 nm) are diminished.
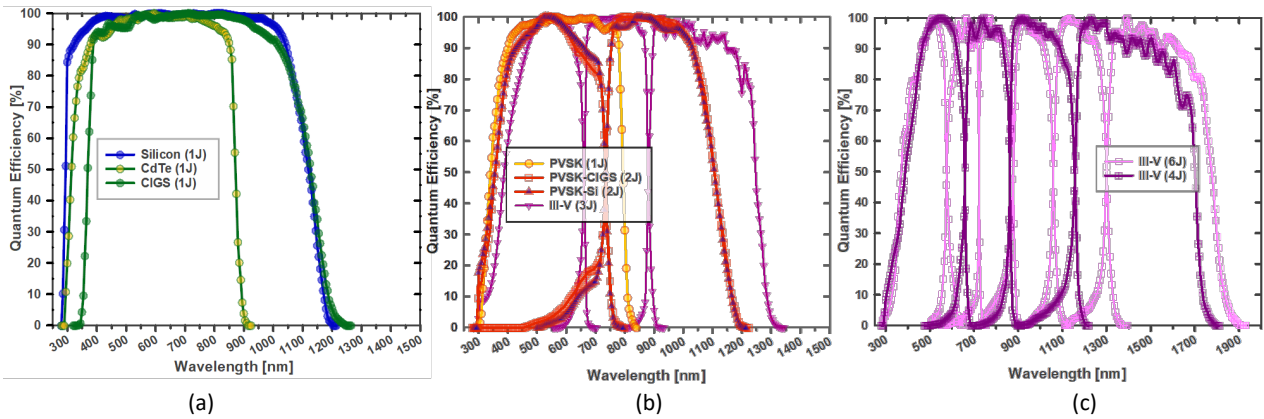

Figure 2. Solar cell quantum efficiencies digitized at 5-nm intervals from the Solar Cell Efficiency Tables: (a) silicon (Si), cadmium telluride (CdTe), and copper indium gallium selenide (CIGS); (b) perovskite (PVSK), perovskite-CIGS tandem (PVSK-CIGS), perovskite-silicon tandem (PVSK-Si), and a three-junction III-V; (c) four-, and six-junction III-Vs.

Analysis

The influence of spectral variation on nine solar cell types is evaluated using their current-best characteristics (Appendix C), as given in the Solar Cell Efficiency Tables[74] and NREL's Best Research-Cell Efficiency Chart[25]. Four single-junction cells (silicon[75], cadmium telluride[76], CIGS[74], and perovskite[77]) are considered, along with five two-terminal multijunctions (perovskite-CIGS[78], perovskite-silicon[78], and three-, four- and six- junction III-Vs[74,76,79]. Multijunctions convert solar energy using two or more semiconductor junctions. Stacking the junctions increases the cell voltage while splitting the conversion of sunlight into current from each junction. The two-terminal configuration implies a series connection, so the overall device current is limited by whichever junction is producing the least current. As a result, two-terminal multijunctions have more sensitivity to spectrum variation.

Efficiencies from the measured spectra are shown in Figure 3, against a backdrop of the confirmed values under AM1.5G (AM1.5D, for III-V multijunctions). The corresponding relative efficiencies are shown in Figure 4. Cells with a single junction (Si, CdTe, CIGS, and PVSK) demonstrate efficiencies clustered about their efficiency under the AM1.5 standard spectrum. As the number of junctions increases, the degree of spectrum sensitivity increases, and the relative efficiencies in Figure 4 drop. For cells with two or more junctions, the performance under AM1.5, rather than being an average value (as with the single-junction cells), tends to be more of an upper bound of the performance seen under measured spectra.
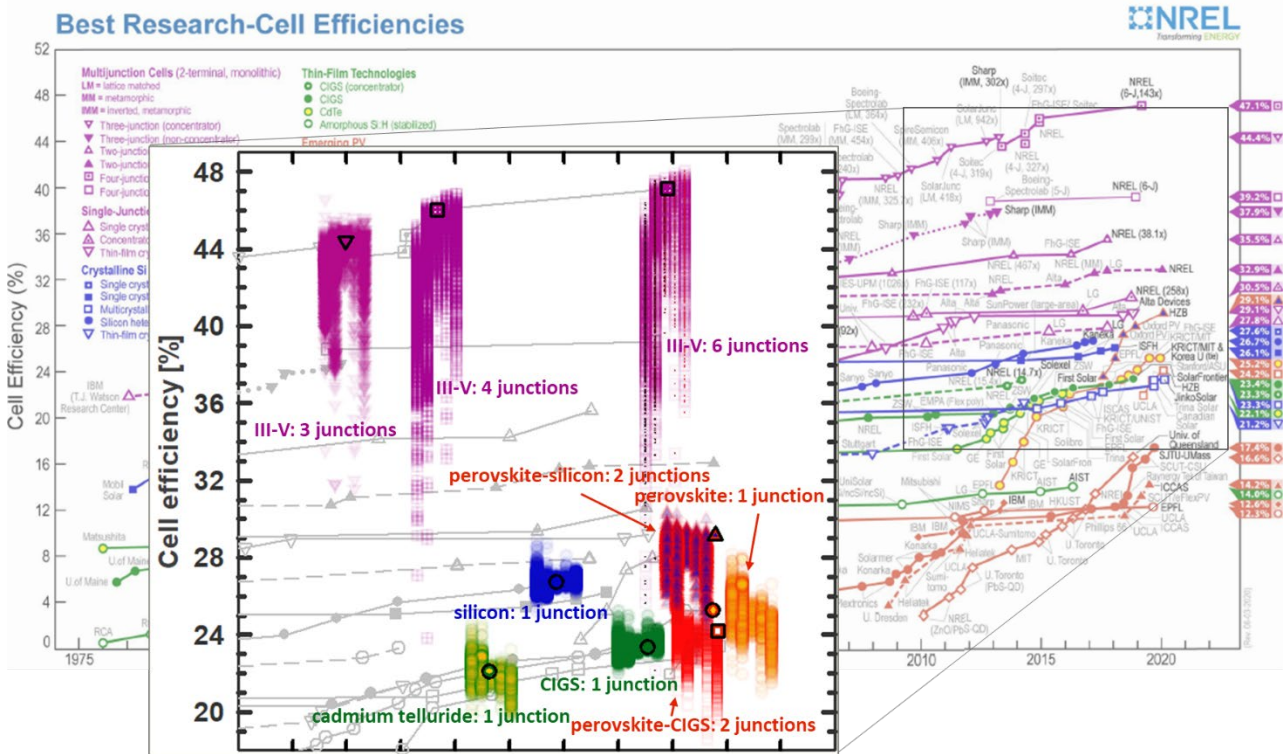
Figure 3. Efficiencies under measured spectral irradiance, compared against the values under Standard Test Conditions (symbols with black border). Symbols are arranged in order of increasing sun tracking: GHI, GTI, G1I, GNI, DNI. Lateral positions are adjusted to improve visibility. Each data point is a weekly sum from spectral irradiance sampled at 10-minute intervals (except for Chajnantor, CHL: 60-minute intervals). Best Research-Cell Efficiency chart courtesy of NREL.
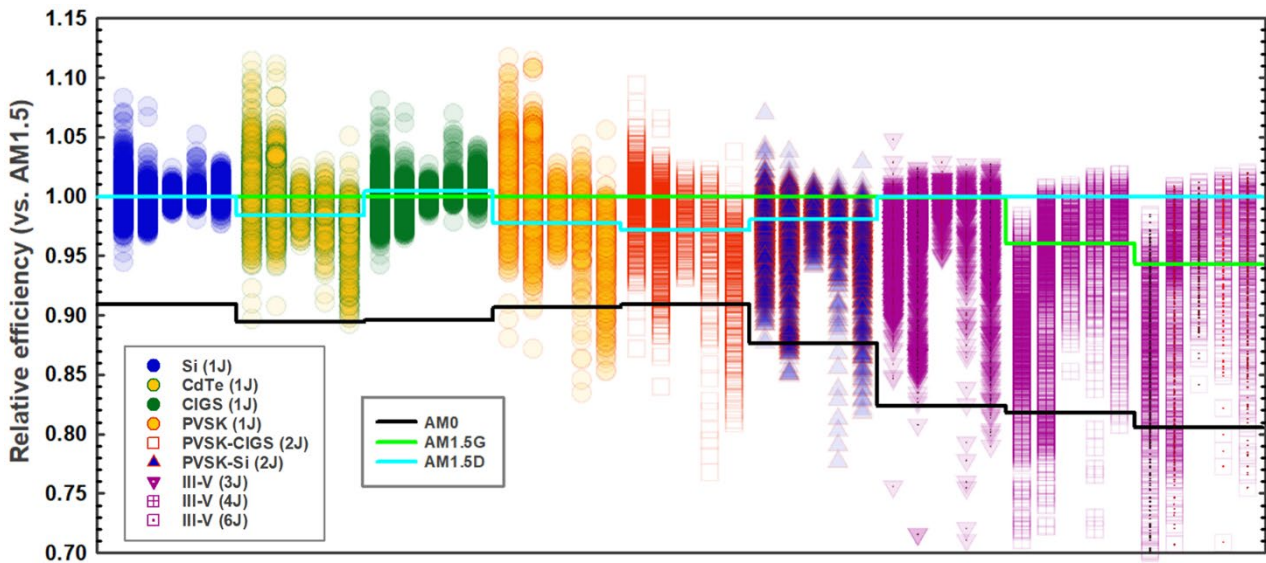

Figure 4. Relative efficiency as a function of cell type and number of junctions: silicon (Si), cadmium telluride (CdTe), CIGS, perovskite (PVSK), perovskite-CIGS tandem (PVSK-CIGS), perovskite-silicon tandem (PVSK-Si), and three-, four, and six-junction III-V multijunctions. For each cell type, data is grouped by orientation: from left to right, GHI, GTI, G1I, GNI, DNI. Lines indicate the relative efficiency of each type under the three standard solar spectra. AM0 is the standard spectrum outside Earth's atmosphere[58]. Each data point is a weekly sum from spectral irradiance sampled at 10-minute intervals (except for Chajnantor, CHL: 60-minute intervals).

Series-connected multijunctions are tuned (by varying the thickness and/or composition of the individual junctions) to optimize current matching of each junction under a given target spectrum. Cells engineered to perform best under AM1.5, therefore, may have been de-tuned from optimum performance in operating conditions. Re-tuning the designs for spectral conditions in operation[80,81] requires different thicknesses and (where possible) material compositions. Designing for operation under AM1.5, alone, may therefore be having an adverse effect on the development of these serially-connected multijunctions. Rating solar efficiency under just a single spectrum is a bit like designing for vehicle efficiency based only on highway driving[82]: it is unlikely to lead to high performance in other conditions.

Consistent with the ratings for temperature and broadband irradiance[16], rating under more than one condition would enable interpolation and extrapolation to other spectral conditions. Figure 4 suggests that AM0, the standard spectrum in space applications[58], could be re-purposed to bracket terrestrial spectrum variation[23]. Fortunately, characterization under two spectra does not require two measurements: if the spectral response of a cell is known, efficiency under a single condition can be translated to that under a second condition using a calculation known as "spectral mismatch correction[83].
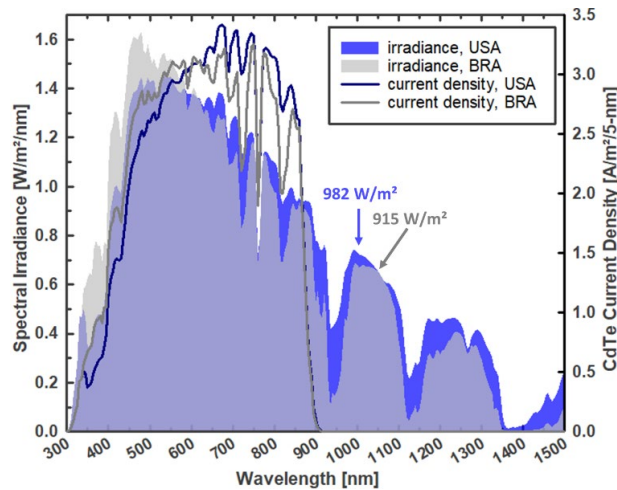

Figure 5. Spectral irradiance and the resulting current density for cadmium telluride from cherry-picked weekly summations found in the Albuquerque (USA) and Sao José dos Campos (BRA) data sets. Cadmium telluride has a spectral response range of ~300-900 nm. The two resulting current density lines form equal areas.

Cells with a wider spectral response (Figure 2) are more tolerant to the increased spectral variation that arises from sun tracking. In Figure 6 and Appendix F, increasing the sun tracking is seen to benefit single-junction cells with a wider spectral response range (silicon, CIGS), but is a detriment to cells with a narrower spectral response (cadmium telluride, perovskites)[23,39,40]. For cells with more than one junction, the result is more mixed, as losses due to current mismatch between the junctions trade against the wider spectral response of the overall stack.

The largest increases in relative efficiency are seen in cells with the narrowest spectral response (cadmium telluride and single-junction perovskite). Since efficiency is the ratio of power out to power in, it should be noted that efficiency rise due to spectrum variation may be due either to an increase in the power provided by the cell, or a decrease in the irradiance outside the cell's spectral response range: higher efficiency does not always imply higher power. This is illustrated in Figure 5, where two spectra are presented that deliver the same output power in a cadmium telluride cell, but different efficiencies. While the broadband irradiance for Albuquerque is 7% higher, the excess falls outside the spectral response range of cadmium telluride. As a result, the two current densities integrate to the same value: 302 A/m², giving a cell output power density of 210 W/m² for both. The efficiency, however, is 21.5% for Albuquerque and 23.0% for Sao José dos Campos.

The fuel transportation costs for solar energy are tough to beat. Inherent variability in the supply, however, brings challenges. Of prime importance to solar array owners, project developers, power plant managers, and grid operators is the variation for their specific location and mounting orientation. Site-specific absolute efficiency values are given in Figure 6. Relative values are given in Figure 7, ranked in order of increasing median efficiency for silicon. The performance of CIGS, with a similar spectral response, follows the increase with silicon; all other efficiencies diverge.

Sample seasonal and diurnal variations are shown in Figure 8. Figures for additional sites, and for annual variation, are included in Appendix F. For the power plant operator, any unexpected variation in power, be it losses or gains, can be costly. Solar power plants employ meteorological ("met") stations to monitor temperature, wind, and plane-of-array (broadband) irradiance. In larger plants, there are often multiple broadband irradiance instruments[84]. In the absence of spectral irradiance monitoring, however, the variation shown in Figure 8 is necessarily confounded with other uncertainties: module and inverter degradation, soiling, cable corrosion, etc.[85] Unexplained losses of a few percent can trigger costly contract disputes or warranty

claims. Conversely, a plant that finds itself with unplanned gains may have to shed that excess power, due to cabling and power electronics that are undersized, or a grid operator unprepared to receive it. Implementing site monitoring procedures for spectral irradiance in line with those established for temperature and broadband irradiance will reduce these losses.
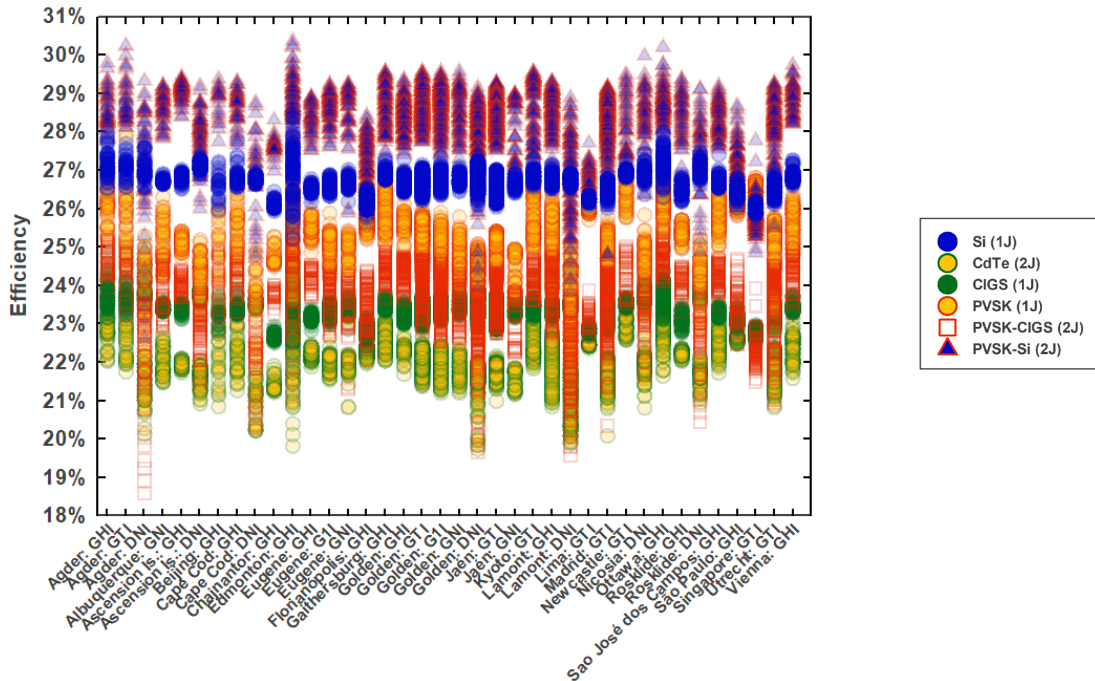

Figure 6. Efficiency as a function of location and orientation for cells with one or two junctions. Results for the III-V multijunctions are included in Appendix D. Each data point is a weekly sum sampled at 10-minute intervals (except for Chajnantor: 60-minute intervals).
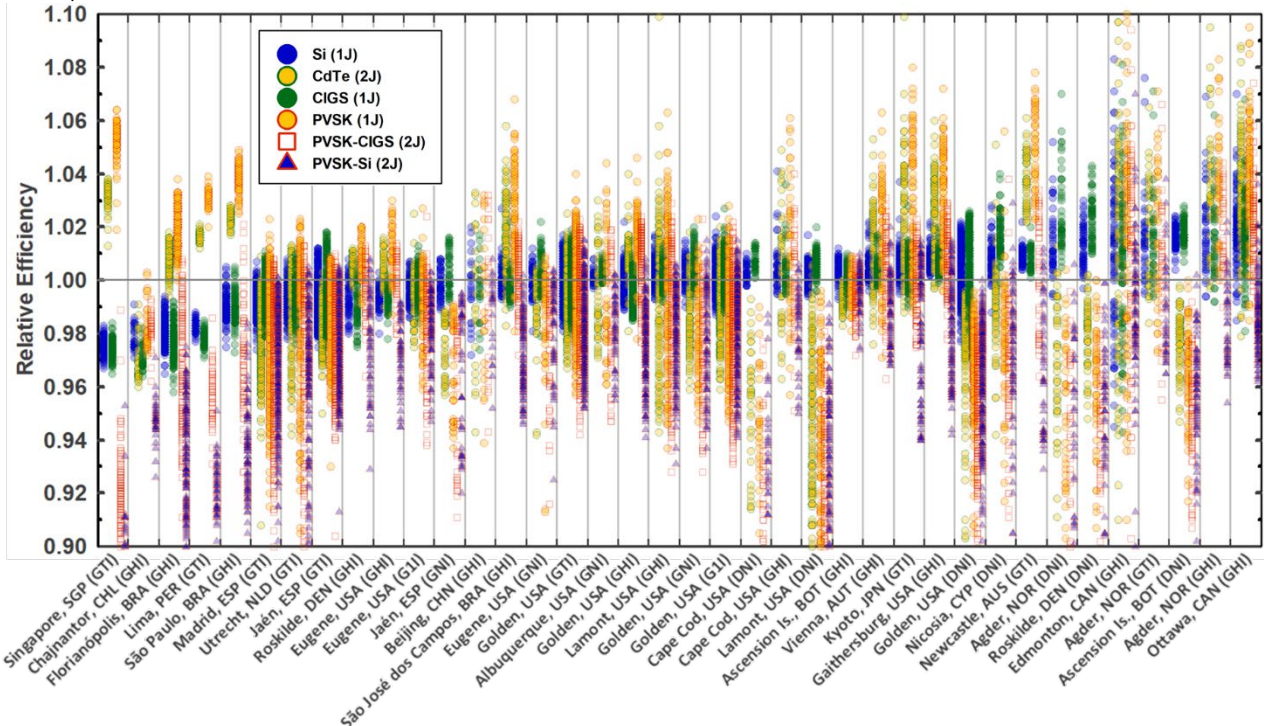

Figure 7. Relative efficiency vs. location and orientation for cells with one or two junctions. Data is sorted by increasing median efficiency of silicon. Location names are approximate. Each data point is a weekly sum from spectral irradiance sampled at 10-minute intervals (except for Chajnantor: 60-minute intervals).

So long as the cost of electricity storage exceeds that of renewable generation[86] and efforts to "electrify everything"[87] to blunt impending climate disruptions continue to gain traction, solar power will be increasingly most valuable at the very times[88] it is most difficult to produce. An (extreme) example is the winter storm that hit the Texas, USA grid in February 2021. Temperatures below freezing caused loss of generation from (insufficiently weatherized) sources that depend on moving parts and the flow of liquids: natural gas, coal,

nuclear, and wind. Winter is not usually considered solar energy's best season, but as other generators dropped offline and electricity prices spiked by factors of more than five[89], solar generation was the only source to deliver increased output[90]. As such, it can be hard to predict exactly when solar energy will be most valuable; efforts to both quantify and minimize daily and seasonal spectral variation losses are needed to maximize the availability and value of solar power to grid operations. Silicon produces the most stable output under spectrum variation: its weekly site-level variation ranges from 1% to 14%, with a mean of 4% (Table 1). Though this is the smallest of the cells evaluated, the mean is equivalent to more than 10° C of temperature variation, or five years of module degradation[91]. Where AM1.5 substitutions were made due to limited measurement range, these are underestimates.
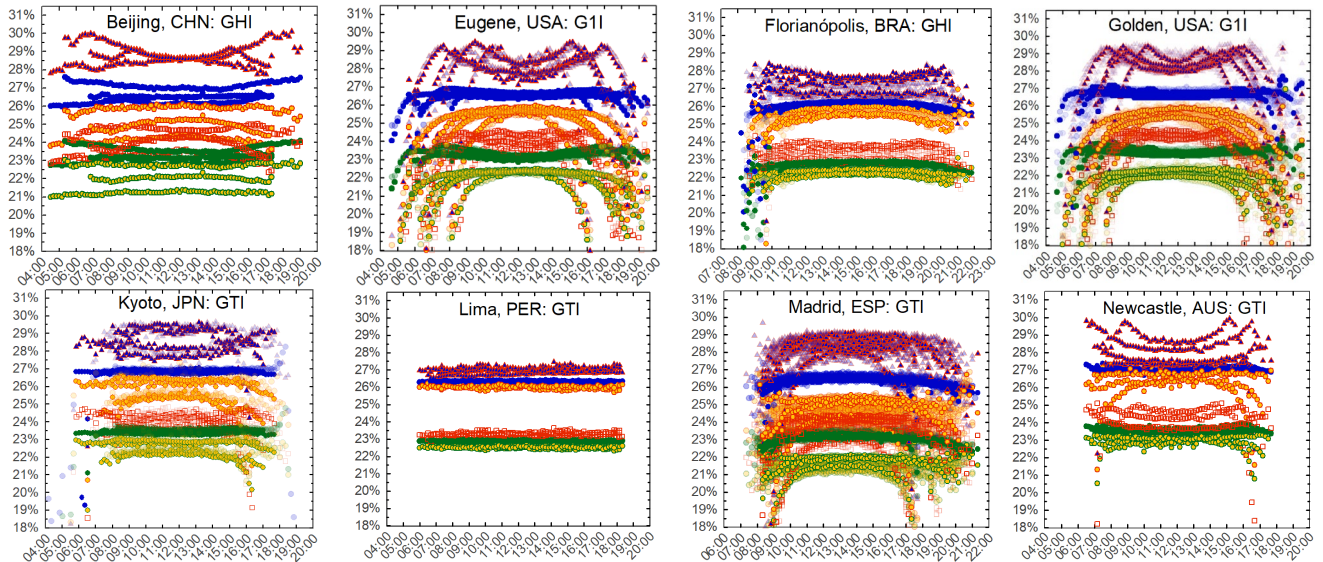

Figure 8. Sample seasonal and diurnal efficiency variations for cells with one or two junctions. Seasonal changes are delineated using one month of data for March, June, September, and December. Where available, data from additional years is semi-transparent in the background. Each data point is a monthly sum. Results for all locations are shown in Appendix F. (Refer to Figure 7 for the legend.)

Conclusion

The measured spectral irradiance data collected here sketches an outline of the spectrum variation affecting solar photovoltaic performance worldwide. Cells with a wider spectral response demonstrate increases in efficiency with increases in sun tracking. Overall, the scale of the impact of spectrum variation on operations argues for expanded monitoring, more in line with that of the other two parameters (temperature and broadband irradiance) that, together, determine solar cell efficiency.

The performance variation indicates that the convention of characterizing under only one spectrum is insufficient for comparison of different cell types. Spectrum sensitivity increases with the number of junctions and efficiency correspondingly declines. For cells with two or more junctions, efficiency under the standard spectrum is closer to a maximum than a representative value: the practice of designing for AM1.5 may be reducing the potential for outdoor operation. Characterization under both AM0 and AM1.5 (for example) would serve to bracket the outdoor performance range, better inform solar cell development, and accelerate deployment.

Table 1. Relative efficiency variation using weekly sums of spectral irradiance at the sensor locations (source shown in brackets). The orientations are global horizontal irradiance (GHI), global tilted irradiance (GTI), global, 1-axis tracking irradiance (G1I), global normal irradiance (GNI), and direct normal irradiance (DNI). Spectral irradiance is sampled at 10-minute intervals (except at Chajnantor: 60-minute) and summed over each week to produce a data point. Location names are approximate.

Cell type (number of junctions):				Silicon (1)	CdTe (1)	CIGS (1)	PVSK (1)	PVSK-CIGS (2)	PVSK-Si (2)	III-V (3)	III-V (4)	III-V (6)
Standard absolute efficiencies:			AM0	24.3%	19.8%	20.9%	22.9%	22.0%	25.6%	36.6%	37.6%	38.0%
			AM1.5G	26.7%	22.1%	23.4%	25.2%	24.2%	29.2%	44.4%	44.2%	44.4%
			AM1.5D	26.7%	21.8%	23.5%	24.6%	23.5%	28.6%	44.4%	46.0%	47.1%
Location & orientation [source]		**Range [nm]**	**Years**					Relative efficiencies $\left(\frac{\eta-\eta_{STC}}{\eta_{STC}}\right)$:				
Agder, NOR [m]	GHI	280-4000	2020	-1% to 7%	0% to 11%	-1% to 6%	0% to 12%	-1% to 4%	-5% to 2%	-15% to 1%	-35% to -6%	-46% to -6%
Agder, NOR [m]	GTI	280-4000	2020	-1% to 8%	-2% to 11%	-1% to 7%	-3% to 11%	-4% to 7%	-4% to 4%	-7% to 2%	-37% to 1%	-48% to 1%
Agder, NOR [m]	DNI	280-4000	2020	-1% to 5%	-9% to 1%	1% to 7%	-16% to 0%	-23% to 0%	-22% to 1%	-29% to 3%	-28% to 2%	-40% to 2%
Albuquerque, USA [92]	GNI	350-1700	2015	0% to 1%	-3% to 3%	0% to 1%	-4% to 4%	-5% to 2%	-5% to 0%	-8% to 1%	-13% to 1%	-14% to 1%
Ascension Island, BOT [93]	GHI	350-1000	2016-2017	-1% to 1%	-2% to 0%	-1% to 1%	-2% to 1%	-3% to 1%	-3% to 1%	-4% to -1%	--	--
Ascension Island, BOT [93]	DNI	350-1000	2016-2017	0% to 2%	-5% to 0%	1% to 3%	-8% to 0%	-12% to -1%	-11% to 0%	-12% to 1%	-10% to 0%	-11% to -1%
Beijing, CHN [s]	GHI	280-4000	2019	-3% to 2%	-6% to 3%	-3% to 2%	-6% to 3%	-6% to 3%	-5% to 1%	-5% to 0%	-12% to -3%	-15% to -3%
Cape Cod, USA [93]	GHI	350-1700	2012-2013	-1% to 4%	-4% to 5%	-1% to 4%	-4% to 6%	-5% to 4%	-5% to 1%	-8% to -1%	-41% to -4%	-51% to -5%
Cape Cod, USA [93]	DNI	350-1700	2012-2013	0% to 1%	-9% to -1%	0% to 1%	-12% to -1%	-16% to -2%	-15% to -1%	-17% to 1%	-16% to 0%	-18% to 0%
Chajnantor, CHL [e]	GHI	290-1800	2016-2017	-3% to -1%	-4% to -1%	-4% to -2%	-3% to 0%	-4% to -1%	-7% to -3%	-11% to -7%	-12% to -9%	-14% to -10%
Edmonton, CAN [n]	GHI	280-4000	2018-2020	-6% to 8%	-10% to 11%	-6% to 8%	-12% to 10%	-13% to 9%	-12% to 7%	-11% to 5%	-35% to -4%	-45% to -4%
Eugene, USA [94]	GHI	350-1050	2020-2021	-2% to 0%	-1% to 2%	-2% to 0%	-1% to 3%	-2% to 1%	-6% to -1%	-5% to 0%	-11% to -3%	-10% to -4%
Eugene, USA [94]	G1I	300-1050	2018-2020	-1% to 1%	-3% to 3%	-2% to 1%	-4% to 3%	-6% to 2%	-5% to 0%	-5% to 1%	-9% to 1%	-7% to 1%
Eugene, USA [94]	GNI	300-1050	2020-2021	-2% to 1%	-6% to 1%	-2% to 2%	-9% to 1%	-12% to 0%	-11% to 0%	-11% to 2%	-9% to 1%	-11% to 1%
Florianópolis, BRA [d]	GHI	295-1100	2018-2020	-4% to -1%	-1% to 2%	-4% to -1%	0% to 4%	-9% to 1%	-12% to -2%	-13% to -2%	-19% to -6%	-20% to -6%
Gaithersburg, USA [95]	GHI	335-1650	2016-2018	0% to 2%	0% to 6%	0% to 2%	0% to 7%	-2% to 3%	-6% to 1%	-14% to 1%	-30% to -6%	-32% to -6%
Golden, USA [81]	GHI	300-1000 / 280-4000	2012-2015 / 2021	-1% to 2%	-2% to 4%	-2% to 2%	-2% to 5%	-2% to 2%	-6% to 1%	-6% to 0%	-18% to -4%	-23% to -4%
Golden, USA [81]	GTI	350-1050	2016-2021	-2% to 2%	-3% to 3%	-2% to 2%	-4% to 4%	-6% to 2%	-5% to 1%	-5% to 2%	-9% to 0%	-7% to -1%
Golden, USA [81]	G1I	350-1650	2016-2021	-1% to 2%	-4% to 2%	-1% to 3%	-5% to 3%	-7% to 2%	-6% to 1%	-5% to 3%	-15% to 1%	-16% to 1%
Golden, USA [81]	GNI	290-1650	2020-2021	-1% to 1%	-4% to 2%	-1% to 2%	-5% to 2%	-7% to 2%	-6% to 1%	-6% to 1%	-14% to 1%	-15% to 1%
Golden, USA [81]	DNI	350-1050	2017-2021	-2% to 2%	-11% to 0%	-2% to 3%	-15% to 0%	-19% to -1%	-18% to 0%	-20% to 1%	-18% to 0%	-22% to 1%
Jaen, ESP [l]	GTI	350-1050	2012-2019	-2% to 1%	-5% to 0%	-3% to 2%	-7% to 1%	-10% to 1%	-9% to 0%	-9% to 1%	-9% to 1%	-9% to 1%
Jaen, ESP [l]	GNI	310-1050	2011-2012	-1% to 1%	-4% to -1%	-1% to 2%	-6% to -1%	-9% to -2%	-8% to -1%	-8% to 1%	-7% to 0%	-9% to 1%
Kyoto, JPN [i]	GTI	300-1700	2018-2020	-1% to 4%	-1% to 10%	-1% to 3%	-1% to 11%	-2% to 2%	-6% to 1%	-19% to 2%	-48% to -2%	-53% to -2%
Lamont, USA [93]	GHI	350-1700	2013-2016	-1% to 2%	-6% to 10%	-1% to 1%	-6% to 10%	-7% to 3%	-7% to 1%	-24% to 1%	-37% to -3%	-34% to -3%
Lamont, USA [93]	DNI	350-1700	2013-2016	-1% to 2%	-10% to 1%	0% to 2%	-15% to 0%	-19% to -2%	-18% to -1%	-21% to 1%	-19% to 1%	-23% to 1%
Lima, PER [q]	GTI	350-1050	2019-2020	-2% to -1%	1% to 2%	-3% to -1%	2% to 4%	-7% to -1%	-10% to -5%	-11% to -5%	-16% to -10%	-16% to -8%
Madrid, ESP [l]	GTI	350-1050	2011-2017	-3% to 1%	-9% to 8%	-3% to 1%	-13% to 11%	-16% to 1%	-15% to 0%	-28% to 0%	-16% to 0%	-15% to 0%
Newcastle, AUS [f]	GTI	280-4000	2017	0% to 2%	2% to 6%	0% to 2%	2% to 8%	-4% to 3%	-7% to 1%	-13% to -2%	-28% to -10%	-29% to -10%
Nicosia, CYP [g]	DNI	280-4000	2017-2018	-1% to 3%	-6% to 5%	0% to 4%	-8% to 6%	-10% to 4%	-10% to 3%	-10% to 3%	-11% to 2%	-13% to 2%
Ottawa, CAN [n]	GHI	280-4000	2018-2020	-2% to 7%	-2% to 9%	-2% to 7%	-2% to 9%	0% to 7%	-4% to 4%	-10% to 1%	-28% to -5%	-42% to -6%
Roskilde, DEN [b]	GHI	300-1050	2020-2021	-2% to 1%	0% to 1%	-3% to 1%	-1% to 2%	-4% to 1%	-7% to 1%	-9% to 1%	-13% to -4%	-11% to -6%
Roskilde, DEN [b]	DNI	300-1050	2020-2021	0% to 3%	-5% to 0%	1% to 4%	-10% to 0%	-16% to -1%	-15% to 0%	-18% to 2%	-17% to 1%	-25% to 2%
São José dos Campos, BRA [k]	GHI	350-1050	2013-2015	-1% to 3%	-2% to 6%	-1% to 2%	-2% to 7%	-3% to 2%	-5% to 0%	-11% to 0%	-3% to -2%	-4% to -2%
São Paulo, BRA [t]	GHI	350-1050	2019	-3% to 0%	2% to 3%	-3% to 1%	3% to 5%	-7% to 2%	-11% to -2%	-12% to -2%	-18% to -8%	-19% to -9%
Singapore, SGP [o]	GTI	350-1050	2019	-3% to -2%	1% to 4%	-3% to -2%	2% to 6%	-11% to -1%	-15% to -5%	-17% to -5%	-23% to -11%	-26% to -11%
Utrecht, NLD [p]	GTI	350-1050	2014-2017	-2% to 1%	-6% to 1%	-2% to 1%	-10% to 2%	-13% to 1%	-12% to 0%	-15% to 2%	-13% to 1%	-16% to 1%
Vienna, AUT [j]	GHI	350-1600	2019-2021	0% to 2%	-2% to 5%	0% to 2%	-3% to 6%	-4% to 3%	-3% to 2%	-10% to 1%	-31% to -2%	-34% to -2%

Appendix

A. Standard spectra

There are three standard solar spectra for space and terrestrial solar applications: AM0, AM1.5D, and AM1.5G. "AM," short for "air mass," is the hypothetical column of air between the sun and the incident surface. AM0 (defined in 1974), is used for solar cells under extraterrestrial radiation (zero air mass). An air mass of one ("AM1") is the condition when the sun is directly overhead. The standard terrestrial spectrum was established by the American Society for Testing and Materials (ASTM) in 1982, at a time when AM1.5 was considered representative of a "typical" solar module: one tilted at a fixed angle of 37° (mid-latitude USA) and pointed due south.

AM1.5D is the ASTM "direct" spectrum for this orientation, intended to represent only the sunlight coming directly from the sun (or its near vicinity). AM1.5D finds practical application in systems using two-axis trackers and optical concentration (lenses or mirrors) to boost solar cells' power and efficiency. These optical concentrators are effective in concentrating only the collimated rays that come directly from the solar disc. The "global" spectrum, AM1.5G, consists of these direct rays, as well as sunlight that has been scattered by the atmosphere and is arriving on the tilted surface from the hemispherical dome of the sky.

B. Substitution of AM1.5 for values outside the measurement range

AM1.5 values are substituted outside the measurement ranges. Other approaches are possible, but the resulting performance variation is therefore a lower bound. Normalization of the weekly spectral irradiance magnitudes was made at either 880 nm or 1050 nm, wavelengths at which atmospheric variation is at a minimum: the difference between AM1.5 and the solar constant in space (AM0) is less than 1% at these wavelengths[58,59]. 1050 nm was used for most locations, but 880 nm was used in cases (Singapore, e.g.) where the atmospheric absorption in the near infrared is substantially higher than for AM1.5, so normalization at 1050 nm could result in anomalous values that exceed AM0. For the four- and six-junction III-Vs, any data for which one or more junctions falls outside the measurement range is excluded from the results.

The sensitivity of the cell performance variation to this method was evaluated using data from the instruments that measure data beyond 1050 nm. Data from 1050-4000 nm was substituted with AM1.5 values; the results are shown in Figure 9.
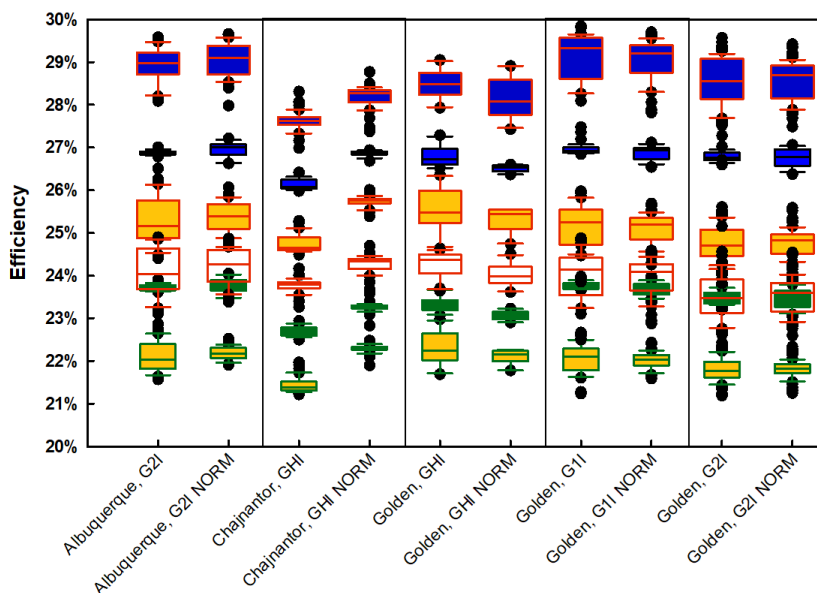

Figure 9. Sensitivity of performance variation to the normalization method. For each site, the left-hand data contains the full measurement range (Table 1); for the right-hand data (labeled "NORM"), measured values beyond 1050 nm have been substituted with AM1.5 values.

C. Calculation of cell efficiency from the quantum efficiency

Cell efficiencies are calculated using the open-circuit voltage (V_{OC}) and fill factor (FF) confirmed under Standard Test Conditions (25° C, 1000 W/m², AM1.5 spectrum). Variations in spectral irradiance are assumed to affect only the cell short-circuit current. Second-order effects, such as changes to voltage or fill factor with changing irradiance[95], or increases in fill factor in multijunctions due to current mismatch[37] are not considered here. The short-circuit current is derived from a cell's spectral response and quantified using the cell quantum efficiency, which is a measure of the percentage of incoming photons at each wavelength that are absorbed and converted into current. Quantum efficiencies obtained from the Solar Cell Efficiency Tables are digitized at 5-nm wavelength intervals. Since the amplitude of the published quantum efficiencies is often normalized, the amplitudes are scaled to obtain the short-circuit current confirmed under the standard spectrum, AM1.5G (AM1.5D, for the III-V multijunctions)[23].

To obtain the current generated under a given spectrum, the spectral irradiance (G_λ) is divided by the photon energy at each wavelength (E_λ) to give the number of photons in that interval (5-nm intervals are used in this study). Multiplying by the quantum efficiency (QE_λ) gives the "spectral current density" [A/m²/nm] that would be converted to current at that wavelength. Multiplying by the wavelength interval ($\Delta\lambda$) yields current density [mA/ cm²] for each interval; summing over all wavelengths obtains the short-circuit current density (J_{SC}):

$$J_{SC} = \sum_{\lambda} \left(\frac{G_\lambda}{E_\lambda}\right) \cdot QE_\lambda \cdot \Delta\lambda$$

The product $V_{OC} \cdot FF \cdot J_{SC}$ is then the cell power density [W/m²]. Dividing by the broadband irradiance [W/m²] obtains the cell efficiency.

Once the quantum efficiency of a given cell type is known, the current density (and cell efficiency) under a standard spectrum can be used to determine the current density under a second spectrum by applying a spectrum mismatch correction[83].
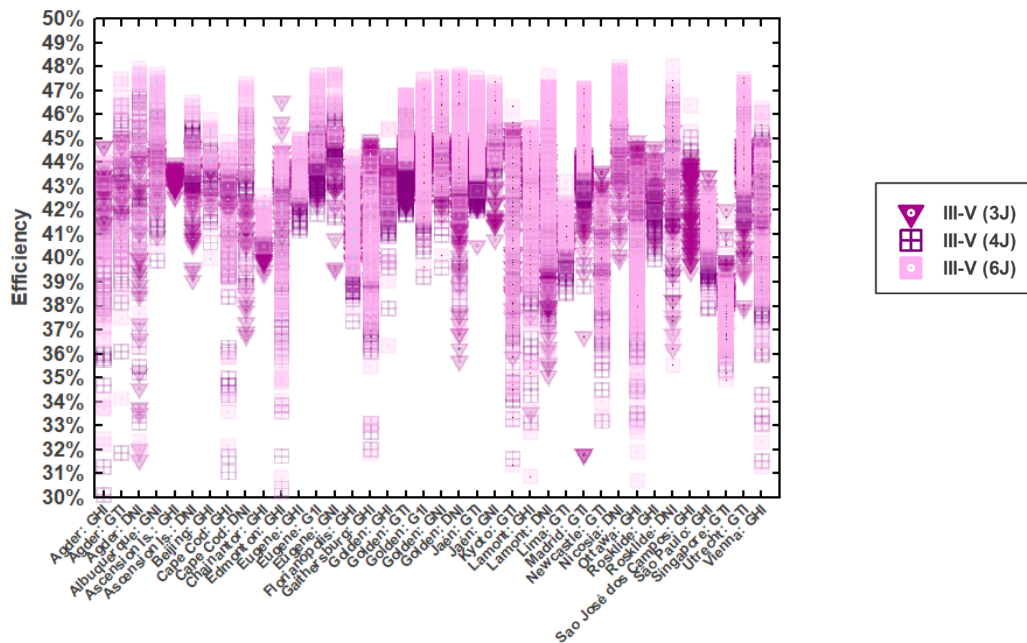
D. Efficiency for III-V multijunctions

Figure 10. Efficiency as a function of location and orientation for III-V multijunction cells.

E. Measured vs. synthetic spectra

Models for solar spectral irradiance enable synthesis of spectral using input atmospheric conditions[63], such as site pressure and the aerosol, water vapor, ozone, and CO_2 levels. Inputs are sourced from both satellite (NOAA/NASA GOES-R) and ground-based atmosphere monitoring instruments. The National Solar Radiation Database at NREL hosts Spectral On-Demand, a tool accessible online as part of the satellite-derived data in the NSRDB Data Viewer[98]. Spectral On-Demand synthesizes spectra within an area defined by NREL's Physical Solar Model[99]. The synthetic spectra below tend to show more irradiance in the visible wavelength range (400-700 nm) than is found in the measured spectra.
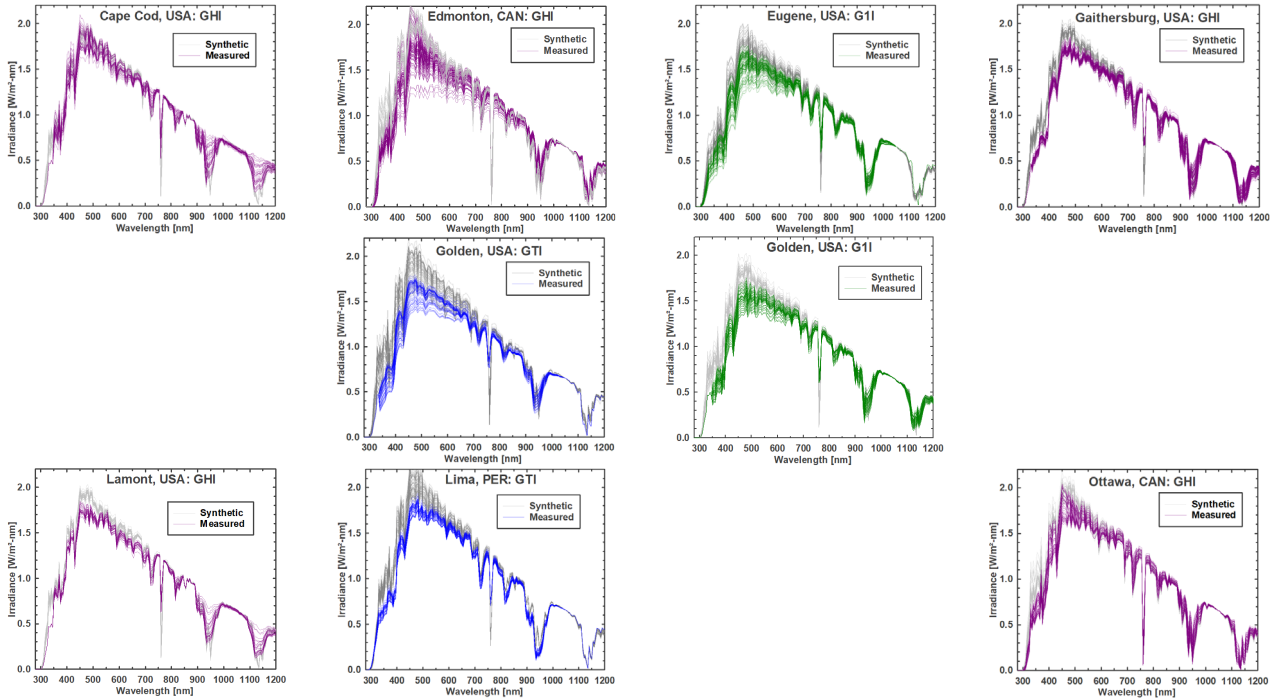

Figure 11. Measured spectra (colors) compared against synthetic spectra (gray) from NREL's Spectral On-Demand.
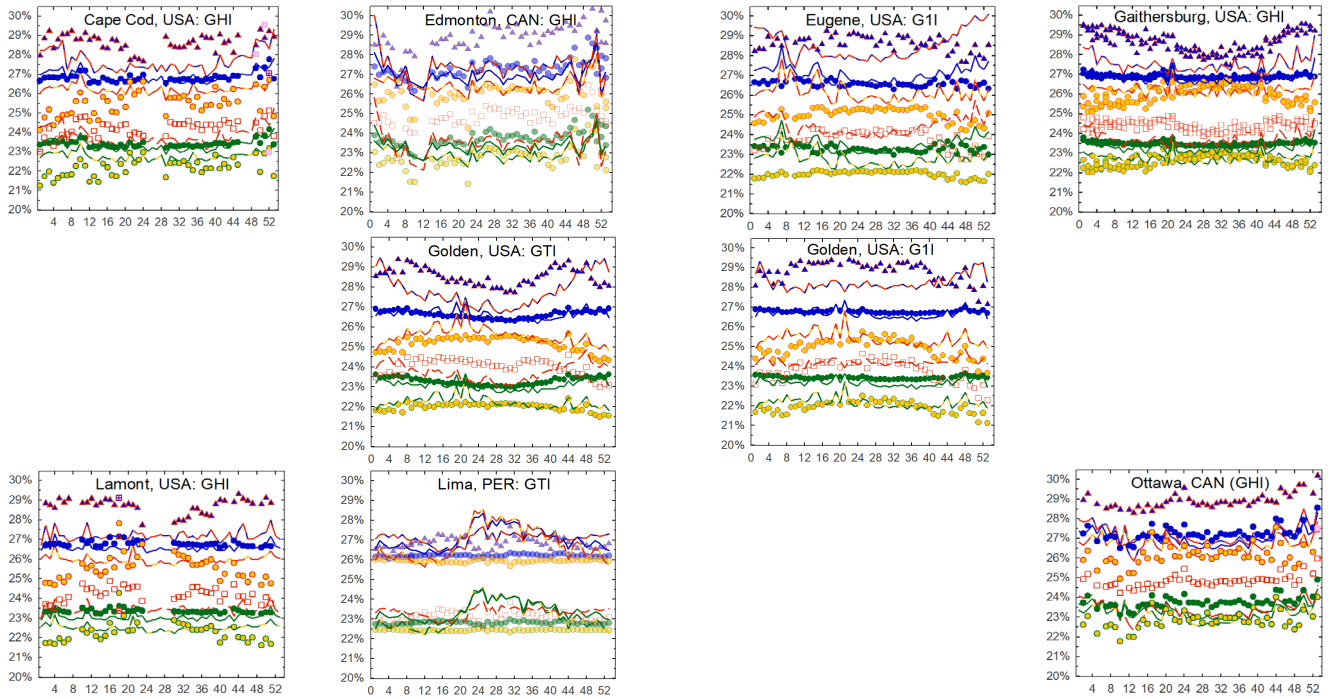

Figure 12. Measured (symbols) vs. synthetic spectra (lines) for sites available from NREL's Physical Solar Model[98] (currently, longitude: -25°E to -175°W, latitude: -20°S to 60°N).

F. Efficiency vs. orientation

As seen in analyses of synthetic spectra[23,39,40], increases in the amount of sun tracking increase the degree of spectral variation and therefore tend to be unfavorable for cells with a narrower spectral response. As the degree of tracking increases in Figure 13 below, efficiency tends to increase for single-junction cells with a wider spectral response (Si, CIGS) and decreases for the cells with a narrower response (CdTe, PVSK).
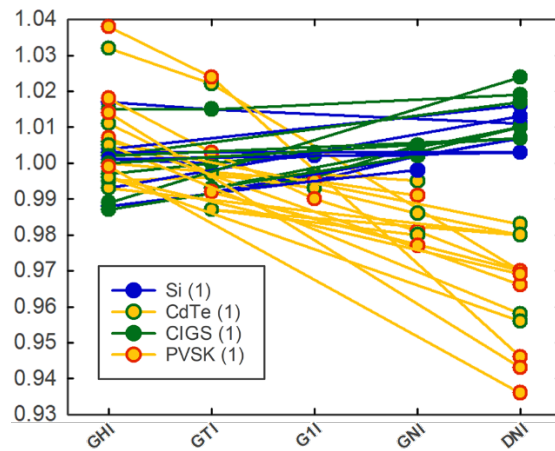

Figure 13. Comparison of relative median efficiency of single-junction cells for sites with more than one sensor orientation: Agder, NOR; Ascension Island, BOT; Cape Cod, USA, Eugene, USA; Golden, USA; Lamont, USA; Jaén, ESP; Roskilde, DEN.

G. Efficiency vs. site latitude

While Figure 7 is suggestive of a relation between site latitude and efficiency, other driving (atmospheric) factors such as site pressure, water vapor, and aerosols are often co-variant with latitude. Latitude, alone, is not a strong predictor of the impact of spectral irradiance variation.
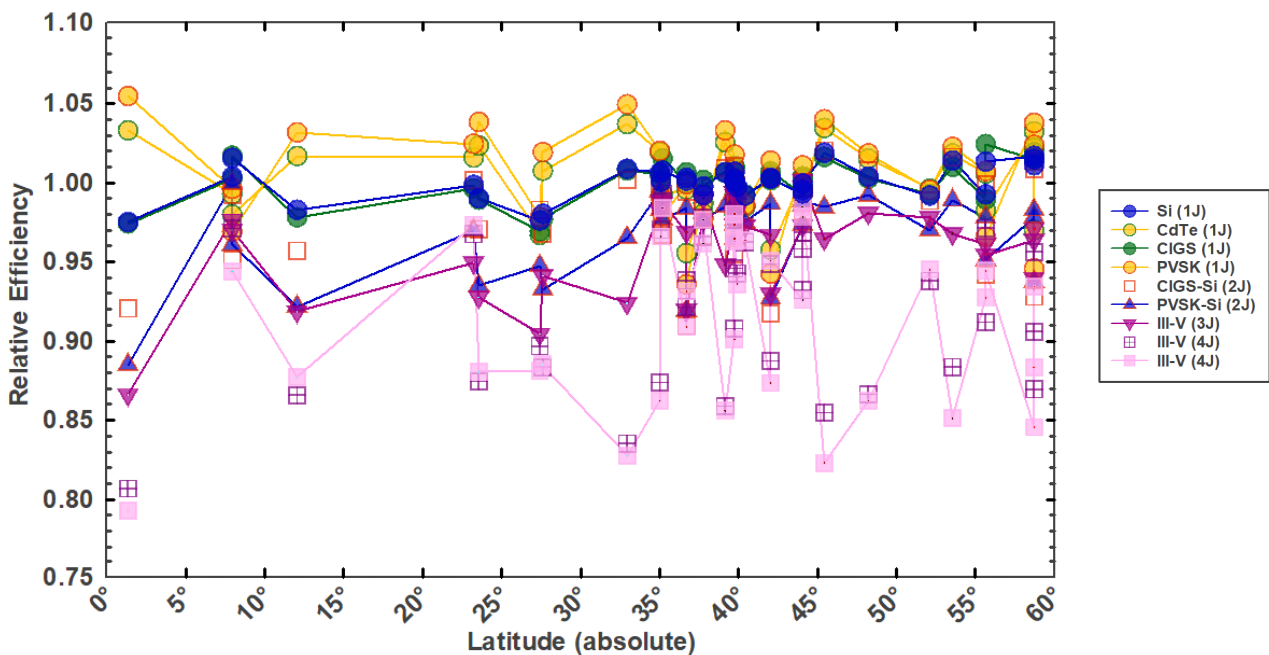
Figure 14. Site median of relative efficiency as a function of the absolute value of site latitude.

H. Diurnal and seasonal variation

Seasonal and diurnal efficiency variations for cells with one or two junctions. Seasonal changes are delineated using one month of data for March, June, September, and December from the most recent year available. Where available, data from prior years is semi-transparent in the background. Data is sampled at 10-minute intervals, except at Chajnantor (60-minute interval). Time basis may be either local or GMT.
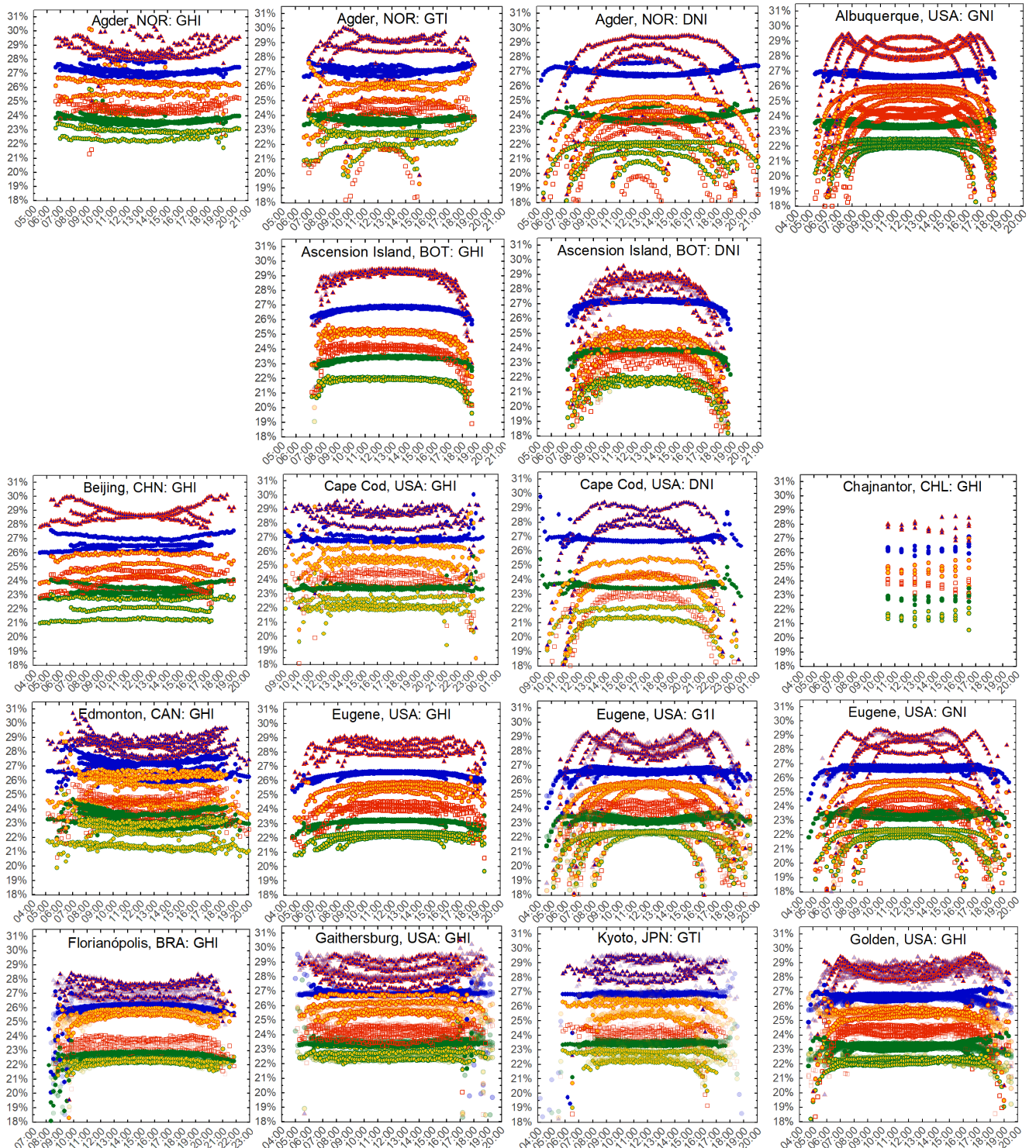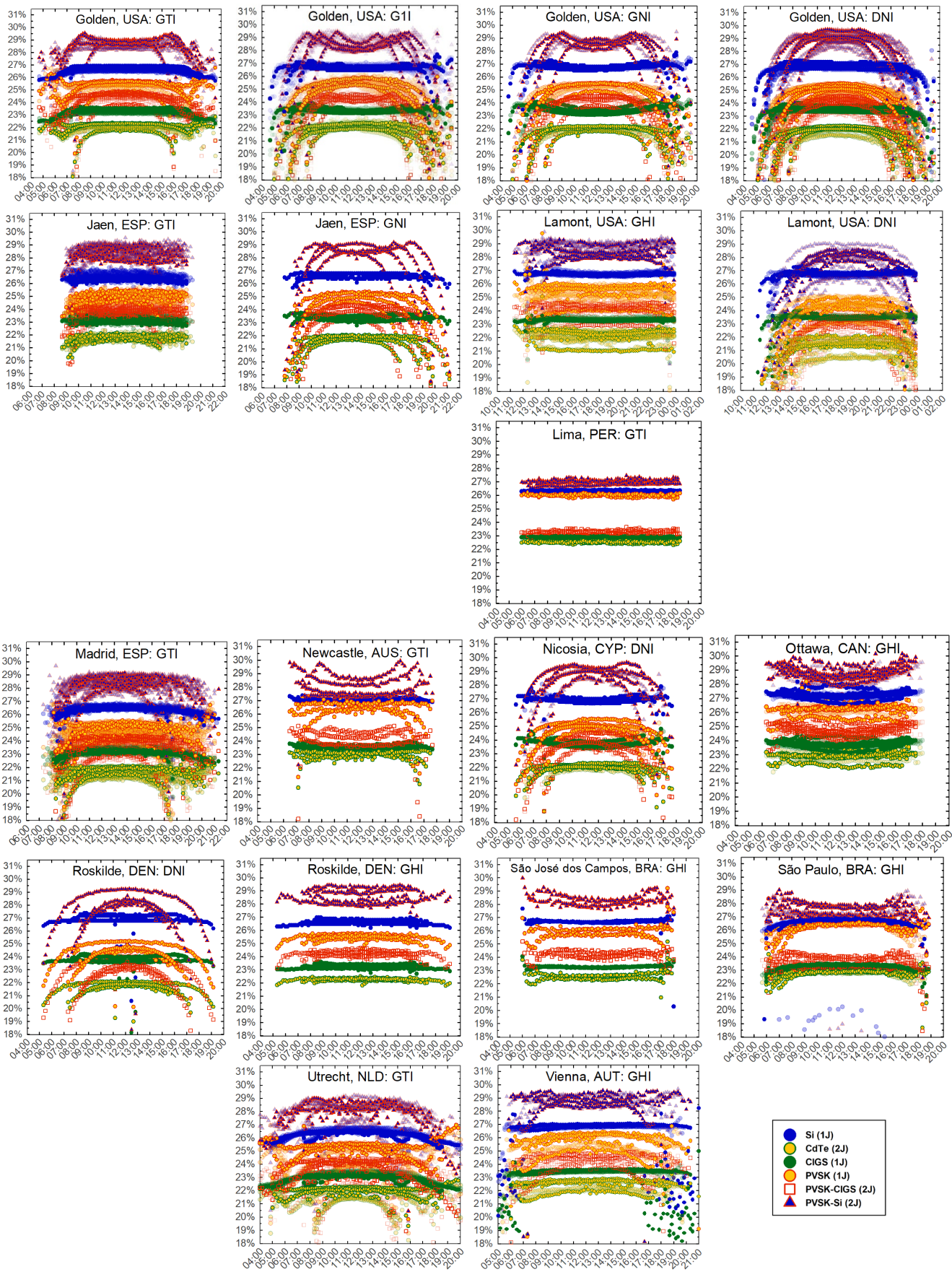
I. Annual efficiency variation: absolute efficiency vs. week of the year for one- and two-junction cells
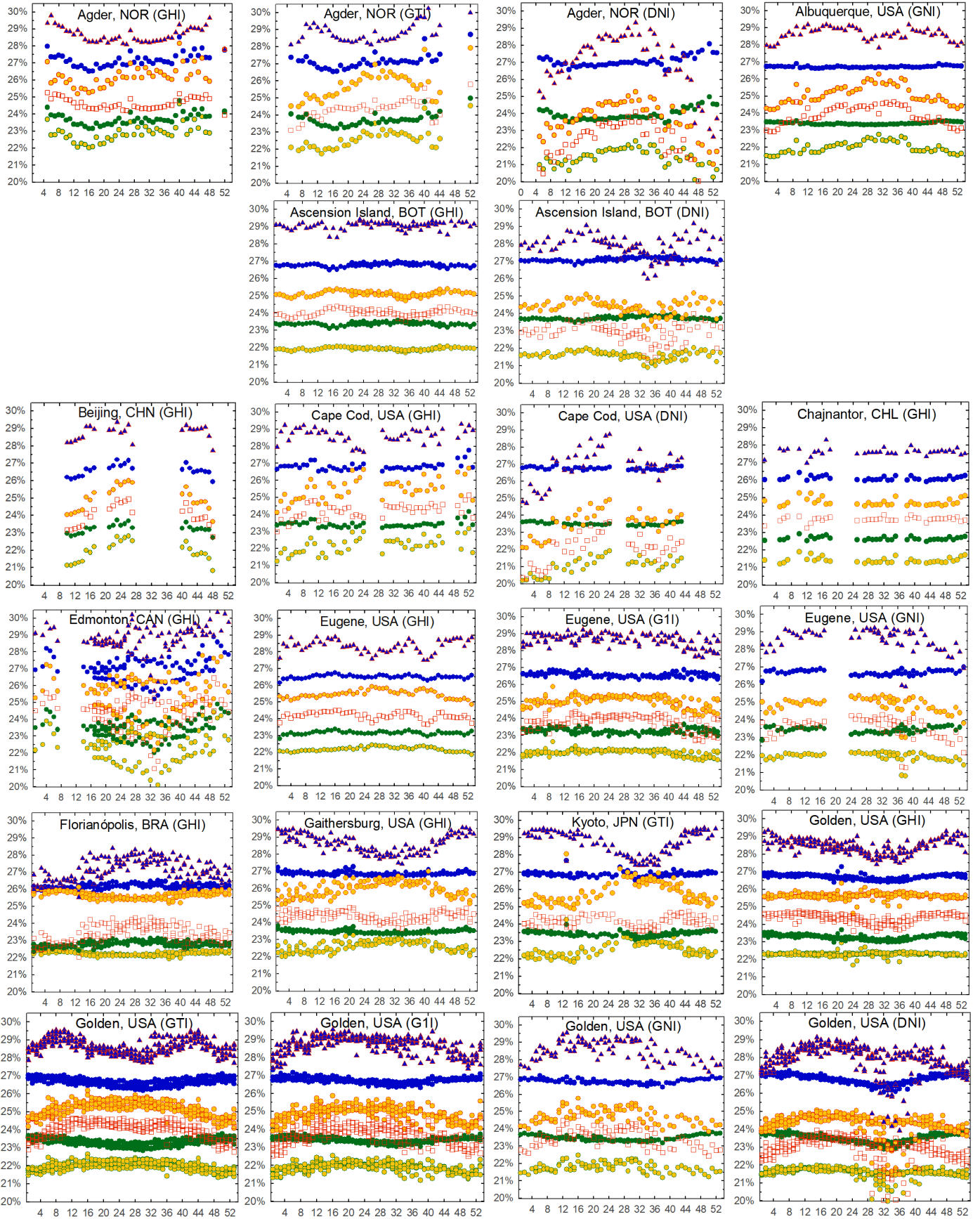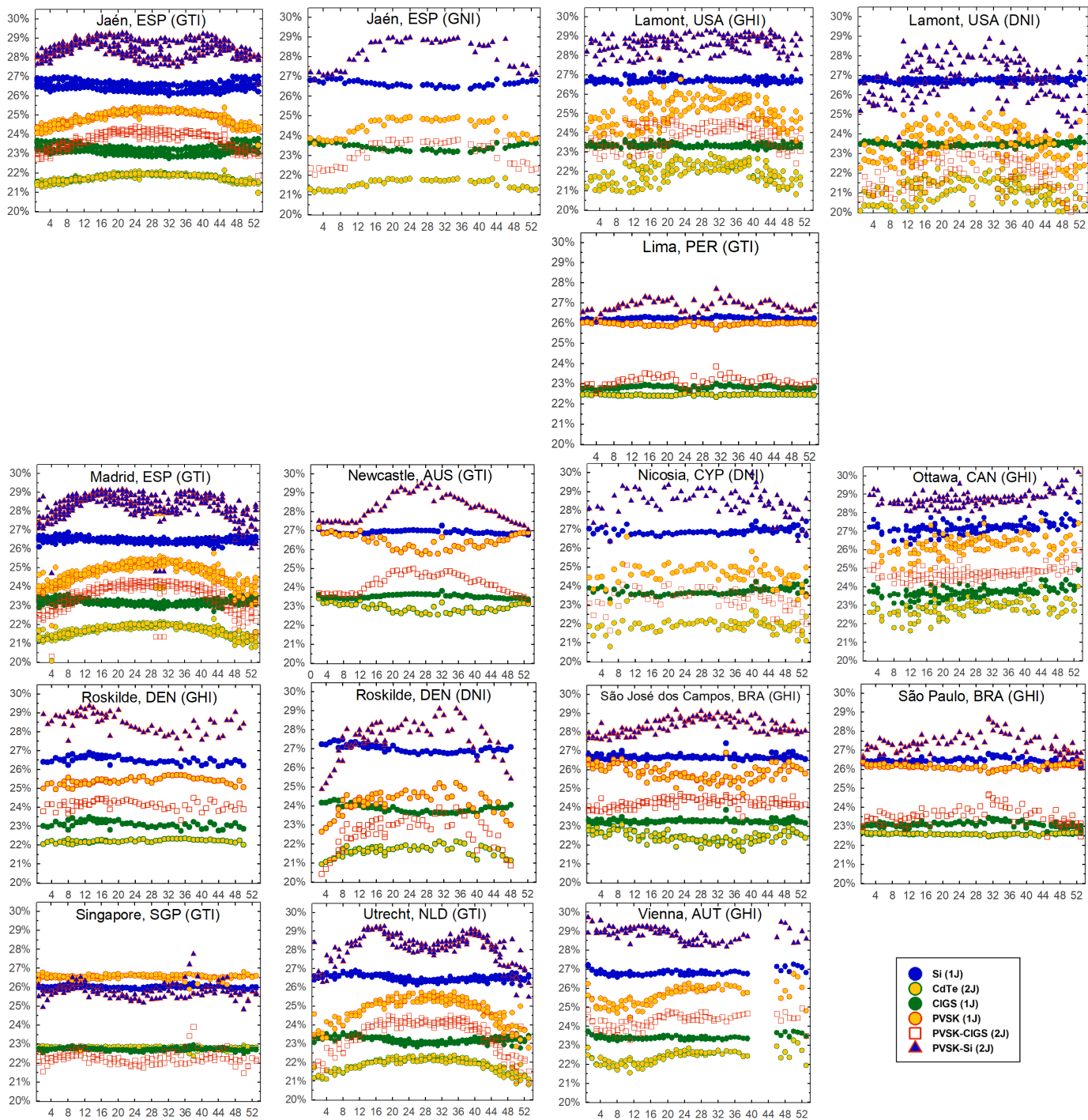
References

1. Faine, P., Kurtz, S. R., Riordan, C. & Olson, J. M. The influence of spectral solar irradiance variations on the performance of selected single-junction and multijunction solar cells. *Solar Cells* **31**, 259–278 (1991).

2. Krauter, S. & Hanitsch, R. Actual optical and thermal performance of PV-modules. *Solar Energy Materials and Solar Cells* **41–42**, 557–574 (1996).

3. Nann, S. & Emery, K. Spectral effects on PV-device rating. *Solar Energy Materials and Solar Cells* (1992) doi:10.1016/0927-0248(92)90083-2.

4. Schweiger, M. Impact of spectral irradiance on energy yield of PV modules measured in different climates. *4th PV Performance Modelling and Monitoring 17 Workshop* (2015) doi:10.13140/RG.2.2.33591.73122.

5. Kinsey, G. S. Spectrum sensitivity, energy yield, and revenue prediction of PV modules. *IEEE Journal of Photovoltaics* **5**, (2015).

6. Nofuentes, G., García-Domingo, B., Muñoz, J. v. & Chenlo, F. Analysis of the dependence of the spectral factor of some PV technologies on the solar spectrum distribution. *Applied Energy* **113**, 302–309 (2014).

7. Minemoto, T., Nagae, S. & Takakura, H. Impact of spectral irradiance distribution and temperature on the outdoor performance of amorphous Si photovoltaic modules. *Solar Energy Materials and Solar Cells* (2007) doi:10.1016/j.solmat.2007.02.012.

8. Myers, D. R., Emery, K. & Gueymard, C. Revising and validating spectral irradiance reference standards for photovoltaic performance evaluation. in *International Solar Energy Conference* (2002). doi:10.1115/SED2002-1074.

9. Hirata, Y. & Tani, T. Output variation of photovoltaic modules with environmental factors—I. The effect of spectral solar radiation on photovoltaic module output. *Solar Energy* **55**, 463–468 (1995).

10. World Energy Outlook 2020 – Analysis - IEA. https://www.iea.org/reports/world-energy-outlook-2020.

11. IEC. IEC 60904-1 Ed. 2.0 b:2006 - Photovoltaic devices - Part 1: Measurement of photovoltaic current-voltage characteristics. *IEC* https://webstore.ansi.org/Standards/IEC/IEC60904Ed2006?gclid=Cj0KCQjw7MGJBhD-ARIsAMZ0eeuLqyJsaU8ouzY8cQhNxdJTJaTpIaxiyA_XhrmcN8dzjFlLhwwzBW0aAsRIEALw_wcB (2006).

12. Reich, N. H. *et al.* Performance ratio revisited: is PR > 90% realistic? *Progress in Photovoltaics: Research and Applications* **20**, 717–726 (2012).

13. NREL. Reference Air Mass 1.5 Spectra | Grid Modernization | NREL. https://www.nrel.gov/grid/solar-resource/spectra-am1.5.html.

14. Wilson, H. R. Effect of solar spectral variation on solar cell short circuit current: results of long-term continuous measurements. *Seventh E.C. Photovoltaic Solar Energy Conference* 309–313 (1987) doi:10.1007/978-94-009-3817-5_57.

15. Riordan, C. & Hulstrom, R. Outdoor spectral solar radiation variations and their relationship to photovoltaic device performance. *Current topics in photovoltaics* 1–23 https://inis.iaea.org/search/search.aspx?orig_q=RN:23072299 (1990).

16. IEC. IEC 60891 Ed. 2.0 b:2009 - Photovoltaic devices - Procedures for temperature and irradiance corrections to measured I-V characteristics. https://webstore.ansi.org/Standards/IEC/IEC60891Ed2009 (2009).

17. Trina Solar. Utility Scale Solar Panels - Trina Solar. https://www.trinasolar.com/us/product/utility (2021).

18. Jinko Solar. *LIMITED WARRANTY*. www.jinkosolar.com (2020).

19. IEC. IEC 61724 Ed. 1.0 b:1998 - Photovoltaic system performance monitoring - Guidelines for measurement, data exchange and analysis. https://webstore.ansi.org/Standards/IEC/IEC61724Ed1998?gclid=Cj0KCQjwpreJBhDvARIsAF1_BU1KSlCweyVqr2NGsnJJEWBJBzH1TJVw28jHUdoGUdo2Bgb9_RMeodQaAgkpEALw_wcB (1998).

20. IEC. IEC 61853-1 Ed. 1.0 b:2011 - Photovoltaic (PV) module performance testing and energy rating - Part 1: Irradiance and temperature performance measurements and power rating. https://webstore.ansi.org/Standards/IEC/IEC61853Ed2011?gclid=CjwKCAjwybyJBhBwEiwAvz4G7zGGe1v53mSa7VebpR9Olf3ZvBe-uj7mNzKvhAxoSPOoTrqdBclnCRoCoqIQAvD_BwE (2011).

21. Solar - Fuels & Technologies - IEA. https://www.iea.org/fuels-and-technologies/solar.

22. Pricing Carbon. https://www.worldbank.org/en/programs/pricing-carbon.

23. Kinsey, G. S. Solar cell efficiency divergence due to operating spectrum variation. *Solar Energy* **217**, 49–57 (2021).

24. Snapshot 2021 - IEA-PVPS. https://iea-pvps.org/snapshot-reports/snapshot-2021/.

25. NREL. Best Research-Cell Efficiency Chart | Photovoltaic Research | NREL. https://www.nrel.gov/pv/cell-efficiency.html (2020).

26. Fernandez, E. F., Cruz, F. A., Mallick, T. K. & Sundaram, S. Effect of Spectral Irradiance Variations on the Performance of Highly Efficient Environment-Friendly Solar Cells. *IEEE Journal of Photovoltaics* (2015) doi:10.1109/JPHOTOV.2015.2434593.

27. Alonso-Abella, M., Chenlo, F., Nofuentes, G. & Torres-Ramírez, M. Analysis of spectral effects on the energy yield of different PV (photovoltaic) technologies: The case of four specific sites. *Energy* (2014) doi:10.1016/j.energy.2014.01.024.

28. Huld, T. & Gracia Amillo, A. M. Estimating PV module performance over large geographical regions: The role of irradiance, air temperature, wind speed and solar spectrum. *Energies* (2015) doi:10.3390/en8065159.

29. Norton, M., Amillo, A. M. G. & Galleano, R. Comparison of solar spectral irradiance measurements using the average photon energy parameter. *Solar Energy* **120**, 337–344 (2015).

30. Dirnberger, D., Blackburn, G., Müller, B. & Reise, C. On the impact of solar spectral irradiance on the yield of different PV technologies. *Solar Energy Materials and Solar Cells* **132**, 431–442 (2015).

31. Cornaro, C. & Andreotti, A. Influence of Average Photon Energy index on solar irradiance characteristics and outdoor performance of photovoltaic modules. *Progress in Photovoltaics: Research and Applications* (2013) doi:10.1002/pip.2194.

32. Ishii, T., Otani, K., Takashima, T. & Xue, Y. Solar spectral influence on the performance of photovoltaic (PV) modules under fine weather and cloudy weather conditions. *Progress in Photovoltaics: Research and Applications* (2013) doi:10.1002/pip.1210.

33. Kinsey, G. S. Spectrum sensitivity, energy yield, and revenue prediction of PV and CPV modules. in *2015 IEEE 42nd Photovoltaic Specialist Conference, PVSC 2015* (2015). doi:10.1109/PVSC.2015.7355850.

34. Lee, M., Ngan, L., Hayes, W. & Panchula, A. F. Comparison of the effects of spectrum on cadmium telluride and monocrystalline silicon photovoltaic module performance. in *2015 IEEE 42nd Photovoltaic Specialist Conference, PVSC 2015* (2015). doi:10.1109/PVSC.2015.7356174.

35. Simon, M. & Meyer, E. L. The effects of spectral evaluation of c-Si modules. *Progress in Photovoltaics: Research and Applications* (2011) doi:10.1002/pip.973.

36. Philipps, S. P. *et al.* Energy harvesting efficiency of III-V triple-junction concentrator solar cells under realistic spectral conditions. *Solar Energy Materials and Solar Cells* (2010) doi:10.1016/j.solmat.2010.01.010.

37. Reynolds, S. & Smirnov, V. Modelling Performance of Two- and Four-terminal Thin-film Silicon Tandem Solar Cells under Varying Spectral Conditions. in *Energy Procedia* (2015). doi:10.1016/j.egypro.2015.12.321.

38. Minemoto, T., Nagae, S. & Takakura, H. Impact of spectral irradiance distribution and temperature on the outdoor performance of amorphous Si photovoltaic modules. *Solar Energy Materials and Solar Cells* **91**, 919–923 (2007).

39. Ripalda, J. M., Chemisana, D., Llorens, J. M. & García, I. Location-Specific Spectral and Thermal Effects in Tracking and Fixed Tilt Photovoltaic Systems. *iScience* **23**, (2020).

40. Kinsey, G. S. *Preprint: Solar cell efficiency divergence due to operating spectrum variation*. https://engrxiv.org/yfx9r/ (2020) doi:10.31224/osf.io/yfx9r.

41. Riedel-Lyngskar, N. *et al.* Spectral Albedo in Bifacial Photovoltaic Modeling: What can be learned from Onsite Measurements? *2021 IEEE 48th Photovoltaic Specialists Conference (PVSC)* 0942–0949 (2021) doi:10.1109/PVSC43889.2021.9519085.

42. Neves, G., Vilela, W., Pereira, E., Yamasoe, M. & Nofuentes, G. Spectral impact on PV in low-latitude sites: The case of southeastern Brazil. *Renewable Energy* **164**, 1306–1319 (2021).

43. Amillo, A. M. G., Huld, T., Vourlioti, P., Müller, R. & Norton, M. Application of satellite-based spectrally-resolved solar radiation data to PV performance studies. *Energies* (2015) doi:10.3390/en8053455.

44. Futscher, M. H. & Ehrler, B. Modeling the Performance Limitations and Prospects of Perovskite/Si Tandem Solar Cells under Realistic Operating Conditions. *ACS Energy Letters* (2017) doi:10.1021/acsenergylett.7b00596.

45. Louwen, A., de Waal, A. C., Schropp, R. E. I., Faaij, A. P. C. & van Sark, W. G. J. H. M. Comprehensive characterisation and analysis of PV module performance under real operating conditions. *Progress in Photovoltaics: Research and Applications* **25**, 218–232 (2017).

46. Braga, M., Rafael Do Nascimento, L. & Rüther, R. *Spectral Impacts on the Performance of mc-Si and New-Generation CdTe Photovoltaics in the Brazilian Northeast*.

47. Conde, L. A. *et al.* Spectral effects on the energy yield of various photovoltaic technologies in Lima (Peru). *Energy* **223**, 120034 (2021).

48. Braga, M., do Nascimento, L. R. & Rüther, R. Spectral modeling and spectral impacts on the performance of mc-Si and new generation CdTe photovoltaics in warm and sunny climates. *Solar Energy* **188**, 976–988 (2019).

49. Sirisamphanwong, C. & Ketjoy, N. Impact of spectral irradiance distribution on the outdoor performance of photovoltaic system under Thai climatic conditions. *Renewable Energy* **38**, 69–74 (2012).

50. Representative identification of spectra and environments (RISE) using k-means - Looney - 2021 - Progress in Photovoltaics: Research and Applications - Wiley Online Library. https://onlinelibrary.wiley.com/doi/10.1002/pip.3358.

51. Looney, E. E. *et al.* Representative identification of spectra and environments (RISE) using k-means. *Progress in Photovoltaics: Research and Applications* **29**, 200–211 (2021).

52. Braga, M., do Nascimento, L. R. & Ruther, R. Spectral Impacts on the Performance of mc-Si and New-Generation CdTe Photovoltaics in the Brazilian Northeast. *Conference Record of the IEEE Photovoltaic Specialists Conference* 1226–1231 (2019) doi:10.1109/PVSC40753.2019.8981152.

53. Magare, D. B. *et al.* Effect of seasonal spectral variations on performance of three different photovoltaic technologies in India. *International Journal of Energy and Environmental Engineering* **7**, (2016).

54. Riedel, N. *et al.* Direct Beam and Diffuse Spectral Irradiance Measurements in a Nordic Country Analyzed with the Average Photon Energy Parameter. *2018 IEEE 7th World Conference on Photovoltaic Energy Conversion, WCPEC 2018 - A Joint Conference of 45th IEEE PVSC, 28th PVSEC and 34th EU PVSEC* 2575–2580 (2018) doi:10.1109/PVSC.2018.8548240.

55. Rüther, R. & Livingstone, J. Seasonal variations in amorphous silicon solar module outputs and thin film characteristics. *Solar Energy Materials and Solar Cells* **36**, 29–43 (1995).

56. Rüther, R., Kleiss, G. & Reiche, K. Spectral effects on amorphous silicon solar module fill factors. *Solar Energy Materials and Solar Cells* **71**, 375–385 (2002).

57. Peters, I. M., Liu, H., Reindl, T. & Buonassisi, T. Global Prediction of Photovoltaic Field Performance Differences Using Open-Source Satellite Data. *Joule* **2**, 307–322 (2018).

58. ASTM. *ASTM E490-00a (2019), Solar Constant and Zero Air Mass Solar Spectral Irradiance Tables*. *ASTM International* (2004).

59. ASTM G173-03. *G173-03(2012) Standard Tables for Reference Solar Spectral Irradiances: Direct Normal and Hemispherical on 37° Tilted Surface*. *ASTM International* (2012).

60. Spectroradiometers | EKO Instruments. https://eko-eu.com/products/solar-energy/spectroradiometers.

61. Tatsiankou, V. *et al.* Extensive validation of solar spectral irradiance meters at the World Radiation Center. *Solar Energy* **166**, 80–89 (2018).

62. Tatsiankou, V., Hinzer, K., Schriemer, H., McVey-White, P. & Beal, R. Efficient, Real-Time Global Spectral and Broadband Irradiance Acquisition. *2018 IEEE 7th World Conference on Photovoltaic Energy Conversion, WCPEC 2018 - A Joint Conference of 45th IEEE PVSC, 28th PVSEC and 34th EU PVSEC* 2362–2365 (2018) doi:10.1109/PVSC.2018.8547671.

63. Gueymard, C. A. SMARTS2: a simple model of the atmospheric radiative transfer of sunshine: algorithms and performance assessment. *Report No. FSEC-PF-270-95* (1995).

64. Myers, D. R. & Gueymard, C. A. Description and availability of the SMARTS spectral model for photovoltaic applications. in *Organic Photovoltaics V* (2004). doi:10.1117/12.555943.

65. Myers, D. R., Emery, K. & Gueymard, C. Terrestrial solar spectral modeling tools and applications for photovoltaic devices. in *Conference Record of the IEEE Photovoltaic Specialists Conference* (2002). doi:10.1109/pvsc.2002.1190943.

66. Xie, Y. & Sengupta, M. A Fast All-sky Radiation Model for Solar applications with Narrowband Irradiances on Tilted surfaces (FARMS-NIT): Part I. The clear-sky model. *Solar Energy* (2018) doi:10.1016/j.solener.2018.09.056.

67. Xie, Y., Sengupta, M. & Wang, C. A Fast All-sky Radiation Model for Solar applications with Narrowband Irradiances on Tilted surfaces (FARMS-NIT): Part II. The cloudy-sky model. *Solar Energy* (2019) doi:10.1016/j.solener.2019.06.058.

68. Kinsey, G. S., Stone, K., Brown, J. & Garboushian, V. Energy prediction of Amonix CPV solar power plants. *Progress in Photovoltaics: Research and Applications* **19**, (2011).

69.   Kinsey, G. S. Weighing the merits of solar power plants using concentration photovoltaics - PV Tech. *PV Tech* https://www.pv-tech.org/technical-papers/weighing-the-merits-of-solar-power-plants-using-concentration-photovoltaics/ (2012).

70.   Kinsey, G. S. *et al.* Advancing efficiency and scale in CPV Arrays. *IEEE Journal of Photovoltaics* **3**, (2013).

71.   Yamasoe, M. A., Artaxo, P., Miguel, A. H. & Allen, A. G. Chemical composition of aerosol particles from direct emissions of vegetation fires in the Amazon Basin: Water-soluble species and trace elements. *Atmospheric Environment* **34**, 1641–1653 (2000).

72.   JD, H., AR, W., R, T. & JW, H. An influence of solar spectral variations on radiative forcing of climate. *Nature* **467**, 696–699 (2010).

73.   Foote, E. Circumstances Affecting the Heat of the Sun's Rays. *The American Journal of Science and Arts, Art. XXXI* 382 https://books.google.co.uk/books?id=fjtSAQAAMAAJ&lpg=PA382&dq="Circumstances Affecting the Heat of the Sun's Rays" foote&pg=PA382 (1856).

74.   Green, M. A. *et al.* Solar cell efficiency tables (Version 53). *Progress in Photovoltaics: Research and Applications* (2019) doi:10.1002/pip.3102.

75.   Green, M. A. *et al.* Solar cell efficiency tables (version 50). *Progress in Photovoltaics: Research and Applications* (2017) doi:10.1002/pip.2909.

76.   Green, M. A., Emery, K., Hishikawa, Y., Warta, W. & Dunlop, E. D. Solar cell efficiency tables (Version 45). *Progress in Photovoltaics: Research and Applications* (2015) doi:10.1002/pip.2573.

77.   Green, M. A. *et al.* Solar cell efficiency tables (Version 55). *Progress in Photovoltaics: Research and Applications* (2020) doi:10.1002/pip.3228.

78.   Green, M. A. *et al.* Solar cell efficiency tables (version 56). *Progress in Photovoltaics: Research and Applications* (2020) doi:10.1002/pip.3303.

79.   Green, M. A., Emery, K., Hishikawa, Y., Warta, W. & Dunlop, E. D. Solar cell efficiency tables (version 42). *Progress in Photovoltaics: Research and Applications* (2013) doi:10.1002/pip.2404.

80.   Kleiss, G. & Bücher, K. The Need for an International Energy Rating Concept for Photovoltaic Modules. *12th EC Photovoltaic Solar Energy Conference* 299 https://www.researchgate.net/publication/282694733_The_need_for_an_International_Energy_Rating_Concept_for_Photovoltaic_Modules (1994).

81.   Raicu, A., Heidler, K., Kleiss, G. & Bücher, K. Realistic reporting conditions -RRC- for site-dependent energy rating of PV devices. in *11th European Photovoltaic Solar Energy Conference* (eds. Communities., C. of the E. & Guimarães, L. (Leopoldo)) 1323–1326 (Harwood Academic, 1993).

82.   Kinsey, G. S. 2021 Photovoltaic Reliability Workshop Poster Session D, "Solar cell efficiencies under operating spectra" D-2 February 25, 2021 - YouTube. https://www.youtube.com/watch?v=Uctmjh06KKQ&t=3240s (2021).

83.   IEC 60904-7. *IEC 60904-7 Edition 3.0 Part 7: Computation of the spectral mismatch correction for measurements of photovoltaic devices*. *International Electrotechnical Commission* (2008).

84.   Kipp & Zonen. *Solar Irradiance Monitoring in Solar Energy Projects*. https://www.kippzonen.com/Download/810/Brochure-Solar-Irradiance-Monitoring-in-Solar-Energy-Projects.

85.   Built solar assets are 'chronically underperforming' and modules degrading faster than expected, research finds - PV Tech. https://www.pv-tech.org/built-solar-assets-are-chronically-underperforming-and-modules-degrading-faster-than-expected-research-finds/.

86. IRENA. Electricity storage and renewables: Costs and markets to 2030. */publications/2017/Oct/Electricity-storage-and-renewables-costs-and-markets.*

87. NREL. Electrification Futures Study: A Technical Evaluation of the Impacts of an Electrified U.S. Energy System | Energy Analysis | NREL. https://www.nrel.gov/analysis/electrification-futures.html.

88. California invested heavily in solar power. Now there's so much that other states are sometimes paid to take it - Los Angeles Times. https://www.latimes.com/projects/la-fi-electricity-solar/.

89. Herscher, R. Texas Electricity Bills Skyrocket Due To Winter Storm : Live Updates: Winter Storms 2021 : NPR. *NPR* https://www.npr.org/sections/live-updates-winter-storms-2021/2021/02/21/969912613/after-days-of-mass-outages-some-texas-residents-now-face-huge-electric-bills (2021).

90. Penney, V. How Texas' Power Generation Failed During the Storm, in Charts - The New York Times. *New York Times* https://www.nytimes.com/interactive/2021/02/19/climate/texas-storm-power-generation-charts.html (2021).

91. SunPower. SunPower product performance. *Products* https://us.sunpower.com/products/solar-panels (2020).

92. Driesse, A. & Stein, J. S. Global normal spectral irradiance in Albuquerque: a one-year open dataset for PV research. *Sandia National Laboratory, SAND2020-12693* https://pvpmc.sandia.gov/modeling-steps/1-weather-design-inputs/irradiance-and-insolation-2/irradiance-data-sources-for-performance-modeling/spectral-irradiance-data-from-albuquerque/ (2020).

93. ARM Research Facility. https://www.arm.gov/.

94. MIDC: University of Oregon (SRML). https://midcdmz.nrel.gov/apps/sitehome.pl?site=UOSMRL.

95. NIST Photovoltaic Data. https://pvdata.nist.gov/.

96. MIDC: NREL Solar Radiation Research Laboratory (BMS). https://midcdmz.nrel.gov/apps/sitehome.pl?site=BMS.

97. Kinsey, G. S. *et al.* Concentrator multifunction solar cell characteristics under variable intensity and temperature. *Progress in Photovoltaics: Research and Applications* **16**, (2008).

98. NREL. NSRDB Data Viewer. *National Renewable Energy Laboratory (NREL)* https://maps.nrel.gov/nsrdb-viewer/?aL=x8CI3i%255Bv%255D%3Dt%26Jea8x6%255Bv%255D%3Dt%26Jea8x6%255Bd%255D%3D1%26VRLt_G%255Bv%255D%3Dt%26VRLt_G%255Bd%255D%3D2%26mcQtmw%255Bv%255D%3Dt%26mcQtmw%255Bd%255D%3D3&bL=clight&cE=0&lR=0&mC=4.740675384778373%2C22.8515625&zL=2.

99. Sengupta, M. *et al.* The National Solar Radiation Data Base (NSRDB). *Renewable and Sustainable Energy Reviews* (2018) doi:10.1016/j.rser.2018.03.003.

AUTHOR AFFILIATIONS:

[a] Zuva Energy, New York, USA. Email: geoffreykinsey@zuvaenergy.com
[b] Department of Photonics Engineering, Technical University of Denmark, Roskilde,Denmark
[c] National Renewable Energy Laboratory, Golden, USA
[d] Laboratório Fotovoltaica/UFSC, Universidade Federal de Santa Catarina (www.fotovoltaica.ufsc.br)
Caixa Postal 476, Florianópolis-SC, 88056-000, Brazil
[e] Departamento de Física, Universidad de Santiago de Chile, Santiago, Chile
[f] CSIRO Energy, 10 Murray Dwyer Circuit, Mayfield West, NSW 2304, Australia
[g] PV Technology Laboratory, FOSS Research Centre for Sustainable Energy, Department of Electrical and Computer Engineering, University of Cyprus, Nicosia 1678, Cyprus
[h] Institute for Renewable Energy, Eurac Research, Viale Druso 1, Bolzano, Italy
[i] Department of Electrical and Electronic Engineering, Ritsumeikan University, 1-1-1 Nojihigashi, Kusatsu, Shiga 525-8577, Japan
[j] Center for Energy, Austrian Institute of Technology - AIT, Vienna, Austria
[k] Brazilian National Institute for Space Research (Instituto Nacional de Pesquisas Espaciais - INPE)
[l] IDEA Research Group, Center for Advanced Studies in Earth Science, Energy and Environment (CEACTEMA), University of Jaén, Campus de Las Lagunillas, 23071-Jaén, Spain
[m] University of Agder, Faculty of Engineering and Sciences, Grimstad, Norway
[n] Natural Resources Canada, Ottawa, Canada
[o] Solar Energy Research Institute of Singapore (SERIS), National University of Singapore (NUS), Singapore 117574, Singapore
[p] Utrecht University, Copernicus Institute of Sustainable Development, Princetonlaan 8A, 3584CB Utrecht, ttne Netherlands
[q] Departamento de Ciencias, Sección Física, Pontificia Universidad Católica Del Perú, Av. Universitaria 1801, 15088, Lima, Perú
[r] Sandia National Laboratories, Albuquerque, NM 87185, USA
[s] Key Laboratory of Middle Atmosphere and Global Environment Observation (LAGEO), Institute of Atmospheric Physics, Chinese Academy of Sciences, Beijing, 100029, China.
[t] Instituto de Física, Universidade de São Paulo, Rua do Matão, Travessa R, 187, CEP 05508-900, São Paulo-SP, Brazil